Published in final edited form as:
Magn Reson Med. 2011 December ; 66(6): 1697–1703. doi:10.1002/mrm.22938.

T_2 Exchange Agents: a New Class of Paramagnetic MRI Contrast Agent That Shortens Water T_2 by Chemical Exchange Rather Than Relaxation

Todd C. Soesbe[1], **Matthew E. Merritt**[1], **Kayla N. Green**[1], **Federico A. Rojas-Quijano**[1], and **A. Dean Sherry**[1,2,*]

[1]Advanced Imaging Research Center, University of Texas Southwestern Medical Center, Dallas, Texas, USA.

[2]Department of Chemistry, University of Texas at Dallas, Dallas, Texas, USA.

Abstract

Exchange of water molecules between the frequency-shifted inner-sphere of a paramagnetic lanthanide ion and aqueous solvent can shorten the T_2 of bulk water protons. The magnitude of the line-broadening T_2 exchange (T_{2exch}) is determined by the lanthanide concentration, the chemical shift of the exchanging water molecule, and the rate of water exchange between the two pools. A large T_{2exch} contribution to the water linewidth was initially observed in experiments involving Eu^{31}-based paramagnetic chemical exchange saturation transfer agents in vivo at 9.4 T. Further in vitro and in vivo experiments using six different Eu^{31} complexes having water exchange rates ranging from zero (no exchange) to 5×10^6 s^{-1} (fast exchange) were performed. The results showed that the exchange relaxivity (r_{2exch}) is small for complexes having either very fast or very slow exchange, but reaches a well-defined maximum for complexes with intermediate water exchange rates. These experimental results were verified by Bloch simulations for two site exchange. This new class of T_{2exch} agent could prove useful in the design of responsive MRI contrast agents for molecular imaging of biological processes.

Keywords

MRI; chemical exchange; water linewidth; T_2 contrast; in vitro; in vivo

Diamagnetic chemical exchange saturation transfer (CEST) agents and paramagnetic CEST (PARACEST) agents use proton spin saturation and water exchange to produce exogenous-based contrast in MR images (1,2). Water protons bound to the inner sphere of a paramagnetic lanthanide ion (Ln ≠ La, Gd, or Lu) are typically shifted well away from the resonance frequency of bulk water protons (3). Radiofrequency saturation at the bound water frequency can produce indirect partial saturation of the bulk water signal through chemical exchange, resulting in negative contrast (i.e., darkening) in regions where the PARACEST agent is present. The percent reduction in bulk water signal is a function of agent concentration, radiofrequency saturation power and duration, and water exchange rate. Paramagnetic complexes can act as PARACEST agents if the water molecule exchange rate is slow when compared with the frequency difference between the two water pools ($k_{ex} << \Delta\omega$) (1,4). One potential advantage of PARACEST agents over Gd-based T_1 agents is that

*Correspondence to: A. Dean Sherry, Ph.D., Advanced Imaging Research Center, University of Texas Southwestern Medical Center, 5323 Harry Hines BLVD, Dallas, Texas 75390-8568. dean.sherry@utsouthwestern.edu.

image contrast can be turned on and off by inserting a frequency-selective radiofrequency saturation pulse before the imaging sequence. This frequency selection creates the potential of imaging multiple lanthanide-based agents simultaneously, each responding to a different physiological parameter or biochemical event. Such agents hold great potential to further extend the functional and molecular imaging capabilities of MR (5). Some published applications of PARACEST include measures of tissue pH (6,7), Zn^{2+} ion concentration (8), beta-cell function (9,10), and the tissue distribution of glucose (11–13).

During initial in vivo studies of Eu^{3+}-based PARACEST agents in mice, we observed a significant loss (>50%) of MR signal in the kidneys (after intravenous injection) and tumors grown from human cancer cell xenografts (after intratumoral injection). This signal loss was present even before a frequency-selective radiofrequency saturation pulse was applied and appeared to be caused by a local decrease in water T_2 because of the presence of the PARACEST agent. Similar phenomena in mouse kidneys were recently observed using a Tm^{3+}-based PARACEST agent and the OPARACHEE (on-resonance paramagnetic agent chemical exchange effect) pulse sequence (14,15). We also observed that this effect was more pronounced when using polymerized versions of the Eu^{3+}-based agents that had higher local concentrations of Eu^{3+} ions and thus more water exchange sites per molecule (16). As the Eu^{3+} ion in these complexes has a relatively small paramagnetic relaxation enhancement when compared with other lanthanide ions (e.g., Gd^{3+}, Tb^{3+}, Dy^{3+} or Tm^{3+}) (17), it was clear that the T_2 line-broadening effect must originate with some other chemical feature of these complexes. This led to the hypothesis that the same slow-to-intermediate water exchange characteristics of these complexes that enable the PARACEST effect can also cause a local decrease in the bulk water signal though T_2 exchange (T_{2exch}).

The effects of chemical exchange with diamagnetic molecules containing exchangeable —NH or —OH protons on transverse relaxation times have been known for over 40 years (18,19). Many early applications focused on using such molecules to suppress the strong water proton signal in high-resolution proton NMR experiments (20–24). Selective reduction of bulk water T_2 by chemical exchange was first proposed as a method for MRI contrast by Aime et al. (25) and has recently been studied in vitro using the —NH-based proton exchange of iopamidol (26). In this article, we have extended this concept to weakly paramagnetic Eu^{3+} agents having variable water exchange rates. Both in vitro relaxation data and in vivo imaging data are presented along with simulations of T_{2exch} using the Bloch equations modified for chemical exchange. It is shown that the transverse relaxivity (r_2) of these agents is a function of water exchange kinetics and that r_2 has a well-defined maximum at a specific exchange rate.

MATERIALS AND METHODS

In Vitro Experiments

The water exchange properties of the six different Eu^{3+} complexes used in this study are summarized in Table 1. The exchange rates were previously determined by fitting CEST-spectra (Z-spectra) of these complexes, taken at several different applied amplitude of (excitation) radiofrequency fields (B_1), to the Bloch equations modified for chemical exchange (17). Five different concentrations of each complex were prepared (e.g., 1.25, 2.5, 5, 10, and 20 mM). The pH and osmolarity for each sample were adjusted to approximately 7.0 and 300 mOsm, respectively. The T_2 of each sample was measured at 0.54 T and 37°C using a Maran Ultra 23 MHz spectrometer, the Carr–Purcell–Meiboom–Gill sequence, and a nonlinear least-squares fitting procedure. The T_2 of each sample was also measured at 9.4 T and 37°C using a Varian 400 MHz vertical bore spectrometer, the Carr–Purcell–Meiboom–Gill sequence, and a nonlinear least-squares fitting procedure.

Bloch Equation Simulations

Simulations of the T_{2exch} contribution to T_2 shortening of the water resonance using the Bloch-McConnell equations were written in MATLAB (MathWorks, Natick, MA). Details of the method were presented by Woessner et al. (27). The M_{xy} components of the magnetization, as predicted by the simulation, were fit to a single exponential decay to yield a T_2 estimate as a function of chemical shift and exchange rate.

In Vivo Experiments

MRI data were acquired on a Varian (Santa Clara, CA) 9.4 T (400 MHz) small animal system using a 38-mm diameter quadrature volume coil. The mice were maintained at 37°C by a flow of warmed air and their temperature was monitored using a rectal thermocouple from Small Animal Instruments (Stony Brook, NY). Images were acquired using a fast spin-echo sequence (pulse repetition time/echo time = 2500/9.12 ms, echo train = 8, average = 4). Each coronal image of the kidneys (128 × 128 × 1 pixel matrix, 38 × 38 × 2 mm field-of-view) had an in-plane resolution of 297 μm and took 3 min to acquire. Three preinjection baseline images were acquired before administration of a 0.25 mmol kg^{-1} dose of agent to the healthy female black six mice via tail vein injection. Images were then continuously acquired (one every 3 min) for 1 hour. A region-of-interest drawn over each kidney was used to measure the mean pixel intensity in each image. Previous PET/CT studies of untargeted Eu^{3+} PARACEST agents (labeled with ^{64}Cu) show that on tail vein injection of similar doses, the kidneys immediately begin to filter the agent from the blood and into the bladder with signal remaining in the kidneys for more than 1 hour (28).

RESULTS

In Vitro Results

Figure 1a shows a plot of transverse relaxation rate (R_2) versus Eu^{3+} concentration (mM) for the six compounds listed in Table 1 collected at 0.54 T (23 MHz) and 37°C. Linear fits were used to calculate the transverse relaxivity (r_2) for each compound. It can be seen that r_2 is small (<0.005 s^{-1} mM^{-1}; Table 1) for compounds with very fast or no water exchange ($EuDOTA^-$ and $EuTETA^-$, respectively) but larger (0.020–0.050 s^{-1} mM^{-1}) for compounds with intermediate water exchange. Figure 1b shows a similar plot for all six compounds collected at 9.4 T (400 MHz) and 37°C. It can be seen that r_2 is again small (<0.055 s^{-1} mM^{-1}) for compounds with very fast or no exchange and larger (0.216–0.527 s^{-1} mM^{-1}) for compounds with intermediate exchange.

There are two notable differences between the data collected at these two B_0 fields. First, the r_2 values at 9.4 T are larger than those at 0.54 T, as expected. The second less obvious, yet highly informative difference is that the order of r_2 for the four intermediate exchange rate compounds is different at the two fields. The latter observation provides new insights into the mechanism and potential uses of such agents for molecular imaging. The reasons for these r_2 differences are thus explained.

The total water proton T_2 (T_{2tot}) of an aqueous solution containing a paramagnetic complex undergoing water chemical exchange is given by:

$$\frac{1}{T_{2\mathrm{tot}}}=\frac{1}{T_{2\mathrm{water}}}+\frac{1}{T_{2\mathrm{para}}}+\frac{1}{T_{2\mathrm{exch}}} \quad [1]$$

where T_{2water} is the transverse relaxation time of pure water and the latter two terms are the paramagnetic (T_{2para}) and exchange (T_{2exch}) contributions due to the paramagnetic ions. Given that the Eu^{3+} ion is only weakly paramagnetic, the $1/T_{2para}$ term can be neglected

except for those situations where the concentration of Eu^{3+} is very high. Equation 1 can then be simplified and rewritten as:

$$\frac{1}{T_{2\text{exch}}} = \frac{1}{T_{2\text{tot}}} - \frac{1}{T_{2\text{water}}} \quad [2]$$

Equation 2 describes all relaxation effects arising from water exchange with the Eu^{3+} ions. The value of $T_{2\text{exch}}$ is described by the Swift–Connick equation (29):

$$\frac{1}{T_{2\text{exch}}} = R_{2\text{exch}} = \frac{P_B}{\tau_B} \cdot \frac{R_{2B}^2 + R_{2B}\tau_B^{-1} + \boldsymbol{\Delta\omega^2}}{\left(R_{2B} + \tau_B^{-1}\right)^2 + \boldsymbol{\Delta\omega^2}}, \quad [3]$$

where R_{2B} is the transverse relaxation rate of the bound water, τ_B is the bound water lifetime, $\Delta\omega$ is the chemical shift difference (in rad s^{-1}) between the two water exchange sites, and P_B is the mole fraction of the paramagnetic ions (e.g., 1 mM/55.5 M). For the limiting case of $\Delta\omega >> R_{2B}$, Eq. 3 reduces to:

$$\frac{1}{T_{2\text{exch}}} = R_{2\text{exch}} = P_B \cdot \frac{\tau_B \boldsymbol{\Delta\omega^2}}{1 + \tau_B^2 \boldsymbol{\Delta\omega^2}} \quad [4]$$

so that $T_{2\text{exch}}$ is now only a function of τ_B, $\Delta\omega$, and P_B (19).

Equation 4 can be used to illustrate the dependence of R_2 on the bound water lifetime (τ_B) for a given molar fraction of paramagnetic ions. By using a 1-mM concentration of paramagnetic ions Eq. 4 can be expressed in terms of exchange transverse relaxivity ($r_{2\text{exch}}$) as a function of τ_B:

$$r_{2\text{exch}} = \left(1.80 \times 10^{-5}\right) \cdot \frac{\tau_B \boldsymbol{\Delta\omega^2}}{1 + \tau_B^2 \boldsymbol{\Delta\omega^2}} \quad [5]$$

A plot of $r_{2\text{exch}}$ versus τ_B (hereafter called a “Swift–Connick” plot based on the assumptions leading to Eq. 5) for Eu^{3+} at 0.54 T ($\Delta\omega$ = 42.5 ppm or 6.14×10^3 rad s^{-1}) is shown in Fig. 2a. The peak in the Swift–Connick plot can be used to delineate fast, intermediate, and slow water exchange regions. It can be seen that for fast and slow exchange rates ($\tau_B < 10^{-6}$ s and $\tau_B > 10^{-2}$ s, respectively) $r_{2\text{exch}}$ approaches zero, while for intermediate exchange rates (10^{-6} s < τ_B < 10^{-2} s) $r_{2\text{exch}}$ reaches a well-defined maximum (0.055 s^{-1} mM^{-1}) at $\tau_B \Delta\omega^{-1}$ (163 μs). The previously measured bound water lifetimes (Table 1) and transverse relaxivities (Fig. 1a) were used to plot markers for the six Eu^{3+} complexes in Fig. 2a. The measured data are in good agreement with the Swift–Connick plot showing that $r_{2\text{exch}}$ is highly dependent on the water exchange rates. Figure 2a predicts that a Eu^{3+} complex with a bound water lifetime of 163 μs at 37°C would have the largest $r_{2\text{exch}}$ at 0.54 T.

A plot of $r_{2\text{exch}}$ versus τ_B for Eu^3 at 9.4 T ($\Delta\omega$ = 42.5 ppm or 1.07×10^5 rad s^{-1}) is shown in Fig. 2b (with the data from 0.54 T superimposed). Figure 2b illustrates that when moving from 0.54 to 9.4 T the maximum $r_{2\text{exch}}$ value increases proportionally (from 0.055 to 0.962 s^{-1} mM^{-1}) with the increase in B_0 and that the bound water lifetime for the maximum $r_{2\text{exch}}$ moves toward faster water exchange (from 163 to 9.4 μs). The reduction in peak τ_B at 9.4 T causes the r_2 relations between the four intermediate compounds to be inverted when compared with the 0.54 T data. The water exchange rates for the four intermediate compounds place them on the rising (or faster) side of the Swift–Connick peak at 0.54 T

(Fig. 2a), while the same water exchange rates place them on the falling (or slower) side of the Swift–Connick peak at 9.4 T (Fig. 2b). This is interesting because it means that while EuDOTA-$(Me_2gly)_4^-$ has the smallest r_2 value of the four intermediate exchange complexes at 0.54 T, it has the largest r_2 value at 9.4 T. Clearly, the experimental data are in good agreement with Swift–Connick theory.

To confirm that the observed variations in transverse relaxivity were due to differences in water exchange rates, r_2 was also measured at different temperatures for two of the six Eu^{3+} compounds studied. Figure 3a shows a plot of transverse relaxation rate (R_2) versus Eu^{3+} concentration (mM) for EuDOTA-$(gly)_4^-$ at three different temperatures collected at 9.4 T. It can be seen that r_2 is proportional to temperature, consistent with EuDOTA-$(gly)_4^-$ being on the falling or "slow" side of the Swift–Connick peak at 9.4 T in Fig. 2b. Figure 3b shows a similar plot for $EuDOTA^-$, where r_2 is now inversely proportional to temperature, consistent with $EuDOTA^-$ being on the rising or "fast" side of the Swift–Connick peak at 9.4 T. The bound water lifetimes (τ_B) predicted by fitting the measured r_2 values to the Swift–Connick peak in Fig. 2b are in agreement with recent exchange rate data for similar EuDOTA-based compounds (30).

Simulation Results

The Bloch-McConnell simulation results were in exact agreement with predictions made by the Swift–Connick equations describing T_2 in exchanging systems, emphasizing the robustness of the Swift–Connick model.

In Vivo Results

Figure 4 shows coronal slices through the kidneys of three different mice before and 30 min after the injection of (a) $EuTETA^-$, (b) EuDOTA-$(gly)_4^-$, and (c) $EuDOTA^-$ (one compound per mouse). During renal clearance of either $EuTETA^-$ or $EuDOTA^-$ (slow and fast exchange, respectively), there was only a slight darkening of the renal pelvis. However, dramatic darkening of the renal pelvis, medulla, and cortex occurred after injection of EuDOTA-$(gly)_4^-$, the intermediate water exchange compound. These contrast effects are readily explained by the differences in water exchange rates and thus r_{2exch} of each compound. These results also explain our prior observations where severe darkening of a tumor occurred after direct injection of a polymeric form of EuDOTA-$(gly)_4^-$ in vivo (16,28). These data provide a benchmark for water exchange conditions that will be required in creating PARACEST agents that can be activated in vivo without producing a significant T_{2exch} effect.

DISCUSSION

The excellent agreement between the experimental in vitro data at both 0.54 T and 9.4 T and the Swift–Connick predictions supports our hypothesis that the negative contrast observed in vivo is largely due to T_2 exchange (T_{2exch}) for Eu^{3+} complexes. As the T_{2exch} effect is concentration dependent, the kidneys are a likely tissue in which to observe this phenomenon as the Eu^{3+} concentration within the renal nephrons is much higher than that of normal vascular space. Also, as the effect depends on B_0, the observed contrast at 9.4 T for a given Eu^{3+} concentration will be significantly reduced at 3.0 T or 1.5 T. This suggests that PARACEST agents with intermediate water exchange rates might be best observed at lower magnetic fields where the T_{2exch} effects are less prominent.

The Swift–Connick equation, giving a simple relationship between r_{2exch} and τ_B as illustrated in Eq. 5, can be used to evaluate water exchange rates for new complexes where

this parameter is unknown. The r_2 of a new compound can be obtained by measuring R_2 as a function of agent concentration (Fig. 1) and the water exchange rate (or τ_B) estimated by finding the intersection of this r_2 on the Swift–Connick plot. The 2-fold degeneracy (i.e., fast or slow side of the Swift–Connick peak) can be resolved by comparison with other similar chemical structures with known bound water lifetimes, measuring the r_2 at two distinct B_0 fields (e.g., 0.54 T and 9.4 T), or by measuring the temperature dependence of r_2 over a small range of temperatures (e.g., ±10°C) (31).

The dependence of r_{2exch} on $\Delta\omega$ can be predicted by plotting the Swift–Connick equation for other lanthanide ions as each ion will have a distinct $\Delta\omega$ for the exchanging water molecule (3). Figure 5 shows that as $\Delta\omega$ increases, the maximum r_{2exch} increases and moves toward faster exchange, with Dy^{3+} giving the largest maximum r_{2exch} (16.3 s^{-1} mM^{-1}) for complexes with fast water exchange (τ_B = 0.8 μs). Chelates of Dy^{3+} (e.g., Dy-DTPA-BMA or sprodiamide) (32) have been proposed as magnetic susceptibility agents in both ex vivo and in vivo studies (32–37), where the concept of T_{2exch} was suggested to explain some of the observed differences when compared with chelates of Gd^{3+} (38,39). Although the theoretical maximum r_{2exch} of a Dy^{3+}-based compound is an order of magnitude less than that of super paramagnetic ion oxide nanoparticles (40), the contrast mechanisms between the two are quite different. Also, by using a paramagnetic rather than a diamagnetic T_{2exch} agent, the same level of contrast can be achieved at much lower concentrations (26).

It should be noted that Fig. 5 illustrates the effect due to r_{2exch} alone. Strongly paramagnetic ions like Ho^{3+}, Tb^{3+}, and Dy^{3+} (where T_{2para} can not be set to zero as in Eq. 2) will also have a paramagnetic transverse relaxivity term (r_{2para}) added to the total r_2. Including the r_{2para} term, which is independent of the exchange rate, would simply shift the Swift–Connick plots for these ions in the positive vertical direction by an amount proportional to their paramagnetic relaxation enhancement (17). Magnetic field inhomogeneity also contributes an additional line-broadening term (effective transverse relaxation time, T_2^*) to T_2 in vivo but this contribution is small when compared with the r_{2exch} contribution for these intermediate-to-slow water exchange Eu^{3+} complexes as illustrated by the in vivo data of Fig. 4. This may not be the case for other lanthanide-based agents such as Dy^{3+}, where T_2^* may play a more significant role.

CONCLUSION

We have presented the first in vitro and in vivo data from weakly paramagnetic Eu^{3+} compounds acting as T_{2exch} contrast agents. We have shown that T_{2exch} contrast is proportional to the water exchange rate and that there is an optimal exchange rate for each paramagnetic lanthanide ion and magnetic field (both determined by $\Delta\omega$). Although the T_{2exch} contrast mechanism is relatively weak when compared with paramagnetic gadolinium T_1 agents or iron oxide T_2* agents, this discovery could nonetheless be useful in the design of new types of molecular imaging agents for MRI. One example would be to create a low molecular weight polymer of a DyDOTA-based agent with an intermediate water exchange rate (r_{2exch} approximately 10–16 s^{-1} mM^{-1} at 9.4 T; Fig. 5) to amplify the T_{2exch} contribution (16). A modest 20-fold degree of polymerization would result in a total molecular r_{2exch} of 200–320 s^{-1} mM^{-1} that would add to the inherent paramagnetic T_2 relaxation effects of Dy^{3+}. By using such an approach, one might be able to create a highly sensitive T_2 contrast agent with an r_2 as comparable with (or even greater than) super paramagnetic ion oxide nanoparticles while retaining the benefits of using a small molecule. We believe this platform could prove useful for detecting cancer-related enzyme activities in vivo.

Acknowledgments

The authors thank Dr. James Ratanakar and Dr. Subha Viswanathan for their assistance with the T_2 measurements and Tomoyasu Mani for synthesizing one of the compounds used in this work.

Grant sponsor: National Institutes of Health; Grant number: RR-02584 and CA-115531; Grant sponsor: Robert A. Welch Foundation; Grant number: AT-584.

REFERENCES

1. Ward KM, Aletras AH, Balaban RS. A new class of contrast agents for MRI based on proton chemical exchange dependent saturation transfer (CEST). J Magn Reson. 2000; 143:79–87. [PubMed: 10698648]
2. Zhang S, Winter P, Wu K, Sherry AD. A novel europium(III)-based MRI contrast agent. J Am Chem Soc. 2001; 123:1517–1518. [PubMed: 11456734]
3. Zhang SR, Sherry AD. Physical characteristics of lanthanide complexes that act as magnetization transfer (MT) contrast agents. J Solid State Chem. 2003; 171:38–43.
4. Woods M, Donald EWC, Sherry AD. Paramagnetic lanthanide complexes as PARACEST agents for medical imaging. Chem Soc Rev. 2006; 35:500–511. [PubMed: 16729144]
5. Weissleder R, Mahmood U. Molecular imaging. Radiology. 2001; 219:316–333. [PubMed: 11323453]
6. Aime S, Barge A, Castelli DD, Fedeli F, Mortillaro A, Nielsen FU, Terreno E. Paramagnetic lanthanide(III) complexes as pH-sensitive chemical exchange saturation transfer (CEST) contrast agents for MRI applications. Magnet Reson Med. 2002; 47:639–648.
7. Aime S, Delli Castelli D, Terreno E. Novel pH-reporter MRI contrast agents. Angew Chem Int Ed. 2002; 41:4334–4336.
8. Trokowski R, Ren J, Kalman FK, Sherry AD. Selective sensing of zinc ions with a PARACEST contrast agent. Angew Chem Int Ed Engl. 2005; 44:6920–6923. [PubMed: 16206314]
9. Woods M, Zhang S, Sherry AD. Toward the design of MR agents for imaging beta-cell function. Curr Med Chem Immunol Endocr Metab Agents. 2004; 4:349–369. [PubMed: 20686642]
10. Lin M, Lubag A, McGuire MJ, Seliounine SY, Tsyganov EN, Antich PP, Sherry AD, Brown KC, Sun XK. Advances in molecular imaging of pancreatic beta cells. Front Biosci. 2008; 13:4558–4575. [PubMed: 18508529]
11. Zhang S, Trokowski R, Sherry AD. A paramagnetic CEST agent for imaging glucose by MRI. J Am Chem Soc. 2003; 125:15288–15289. [PubMed: 14664562]
12. van Zijl PC, Jones CK, Ren J, Malloy CR, Sherry AD. MRI detection of glycogen in vivo by using chemical exchange saturation transfer imaging (glycoCEST). Proc Natl Acad Sci USA. 2007; 104:4359–4364. [PubMed: 17360529]
13. Ren J, Trokowski R, Zhang S, Malloy CR, Sherry AD. Imaging the tissue distribution of glucose in livers using a PARACEST sensor. Magn Reson Med. 2008; 60:1047–1055. [PubMed: 18958853]
14. Jones CK, Li AX, Suchy M, Hudson RHE, Menon RS, Bartha R. In vivo detection of PARACEST agents with relaxation correction. Magnet Reson Med. 2010; 63:1184–1192.
15. Vinogradov E, Zhang SR, Lubag A, Balschi JA, Sherry AD, Lenkinski RE. On-resonance low B-1 pulses for imaging of the effects of PARACEST agents. J Magn Reson. 2005; 176:54–63. [PubMed: 15979362]
16. Wu YK, Zhou YF, Ouari O, Woods M, Zhao PY, Soesbe TC, Kiefer GE, Sherry AD. Polymeric PARACEST agents for enhancing MRI contrast sensitivity. J Am Chem Soc. 2008; 130:13854–13855. [PubMed: 18817395]
17. Viswanathan S, Kovacs Z, Green KN, Ratnakar SJ, Sherry AD. Alternatives to gadolinium-based metal chelates for magnetic resonance imaging. Chem Rev. 2010; 110:2960–3018. [PubMed: 20397688]
18. Leigh JS. Relaxation times in systems with chemical exchange: some exact solutions. J Magn Reson. 1971; 4:308–311.

19. Granot J, Fiat D. Effect of chemical exchange on transverse relaxation rate of nuclei in solution containing paramagnetic-ions. J Magn Reson. 1974; 15:540–548.
20. Bryant RG, Eads TM. Solvent peak suppression in high-resolution NMR. J Magn Reson. 1985; 64:312–315.
21. Rabenstein DL, Fan S, Nakashima TT. Attenuation of the water resonance in Fourier-transform H-1-NMR spectra of aqueous-solutions by spin spin relaxation. J Magn Reson. 1985; 64:541–546.
22. Eads TM, Kennedy SD, Bryant RG. Solvent suppression in high-resolution proton nuclear-magnetic-resonance based on control of trans-verse relaxation rate. Anal Chem. 1986; 58:1752–1756. [PubMed: 3752509]
23. Rabenstein DL, Fan S. Proton nuclear magnetic resonance spectroscopy of aqueous solutions: complete elimination of the water resonance by spin-spin relaxation. Anal Chem. 1986; 58:3178–3184. [PubMed: 3028216]
24. Connor S, Nicholson JK, Everett JR. Chemical exchange and paramagnetic T_2 relaxation agents for water suppression in spin-echo proton nuclear magnetic resonance spectroscopy of biological fluids. Anal Chem. 1987; 59:2885–2891. [PubMed: 3434814]
25. Aime S, Nano R, Grandi M. A new class of contrast agents for magnetic resonance imaging based on selective reduction of water T_2 by chemical exchange. Invest Radiol. 1988; 23:S267–S270. [PubMed: 3198360]
26. Aime S, Calabi L, Biondi L, De Miranda M, Ghelli S, Paleari L, Rebaudengo C, Terreno E. Iopamidol: exploring the potential use of a well-established X-ray contrast agent for MRI. Magnet Reson Med. 2005; 53:830–834.
27. Woessner DE, Zhang SR, Merritt ME, Sherry AD. Numerical solution of the Bloch equations provides insights into the optimum design of PARACEST agents for MRI. Magnet Reson Med. 2005; 53:790–799.
28. Soesbe, TC.; Wu, Y.; Hao, G.; Sun, X.; Sherry, AD. In vivo MR and PET imaging of a highly sensitive polymeric PARACEST contrast agent.. ISMRM Annual Meeting, Molecular & Cellular Probes session; Honolulu, HI. Apr. 2009;
29. Swift TJ, Connick RE. NMR-relaxation mechanisms of O17 in aqueous solutions of paramagnetic cations and the lifetime of water molecules in the first coordination sphere. J Chem Phys. 1962; 37:307–321.
30. Dixon WT, Ren JM, Lubag AJM, Ratnakar J, Vinogradov E, Hancu I, Lenkinski RE, Sherry AD. A concentration independent method to measure exchange rates in PARACEST agents. Magnet Reson Med. 2010; 63:625–632.
31. Terreno E, Castelli DD, Cravotto G, Milone L, Aime S. Ln(III)-DOTAMGIY complexes: a versatile series to assess the determinants of the efficacy of paramagnetic chemical exchange saturation transfer agents for magnetic resonance imaging applications. Invest Radiol. 2004; 39:235–243. [PubMed: 15021328]
32. Roberts TPL, Kucharczyk J, Cox I, Moseley ME, Prayer L, Dillon W, Bleyl K, Harnish P. Sprodiamide injection enhanced magnetic resonance imaging of cerebral perfusion: phase I clinical trial results. Invest Radiol. 1994; 29:S24–S26. [PubMed: 7928245]
33. Rocklage SM, Moseley ME, Kucharczyk J, Norman D, Quay SC. Early detection of perfusion deficits caused by regional cerebral ischemia in cats: T_2 weighted magnetic susceptibility MRI using a nonionic dysprosium contrast agent. Invest Radiol. 1990; 25:S37–S38. [PubMed: 2283250]
34. Nilsson S, Wikstrom G, Ericsson A, Wikstrom M, Oksendal A, Waldenstrom A, Hemmingsson A. Myocardial cell death in reperfused and nonreperfused myocardial infarctions: MR imaging with dysprosium-DTPA-BMA in the pig. Acta Radiol. 1996; 37:18–26. [PubMed: 8611317]
35. Nilsson S, Wikstrom G, Ericsson A, Wikstrom M, Oksendal A, Waldenstrom A, Hemmingsson A. Double-contrast MR imaging of reper-fused porcine myocardial infarction: an experimental study using Gd-DTPA-BMA and Dy-DTPA-BMA. Acta Radiol. 1996; 37:27–35. [PubMed: 8611319]
36. Wang C, Sundin A, Ericsson A, BachGansmo T, Hemmingsson A, Ahlstrom H. Dysprosium-enhanced MR imaging for tumor tissue characterization: an experimental study in a human xenograft model. Acta Radiol. 1997; 38:281–286. [PubMed: 9093166]

37. Zhao SH, Revel D, Arteaga C, Canet E, Liu SZ, Hadour G, Forrat R, Oksendal A. Magnetic susceptibility of Dy-DTPA-BMA to reperfused myocardial infarction in an excised dog heart model: evidence of viable myocardium. Chinese Med J. 2000; 113:260–264.

38. Kellar KE, Fossheim SL, Koenig SH. Magnetic field dependence of solvent proton relaxation by solute dysprosium(III) complexes. Invest Radiol. 1998; 33:835–840. [PubMed: 9818318]

39. Banci, L.; Bertini, I.; Luchinat, C. Nuclear and electron relaxation. VCH; Weinheim: 1994.

40. Tsai Z-T, Wang J-F, Kuo H-Y, Shen C-R, Wang J-J, Yen T-C. In situ preparation of high relaxivity iron oxide nanoparticles by coating with chitosan: a potential MRI contrast agent useful for cell tracking. J Magn Magn Mater. 2010; 322:208–213.

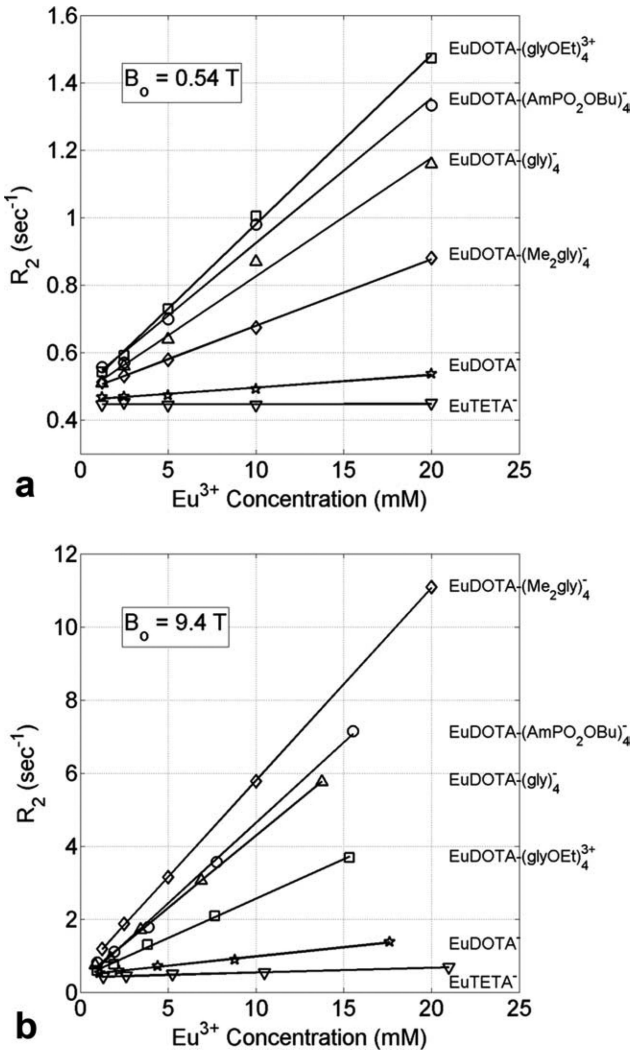

FIG. 1.

a: Transverse relaxation rate (R_2) versus Eu^{3+} concentration (mM) for the six different Eu^{3+} compounds at 0.54 T (23 MHz) and 37°C. **b**: The same data taken at 9.4 T (400 MHz) and 37°C. Each compound has a different water exchange rate (C_B) as shown in Table 1. The slope of each linear fit gives the transverse relaxivity (r_2) for the compound at that B_0.

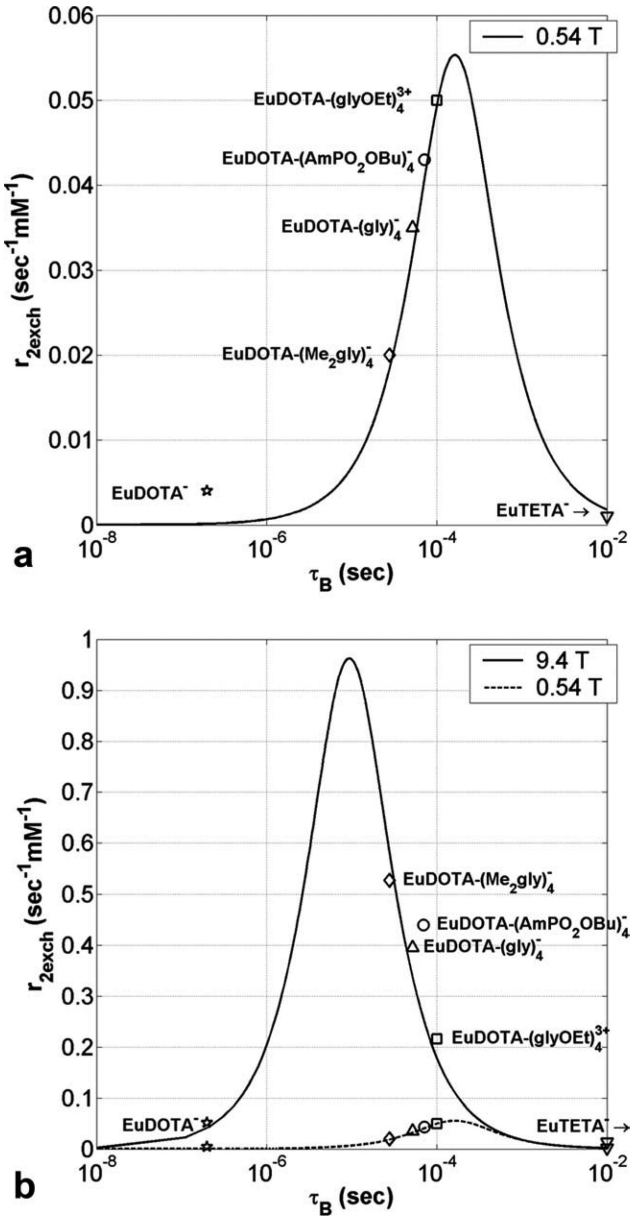

FIG. 2.

a: Transverse relaxivity (s^{-1} mM^{-1}) versus bound water lifetime τ_B (s) for Eu^{3+} at 0.54 T and 37°C as predicted by the Swift–Connick equation (Eq. 5) showing a maximum r_{2exch} of 0.055 s^{-1} mM^{-1} at 163 μs. **b**: The same data but now at 9.4 T. The maximum r_{2exch} is now 17.4 times larger and occurs at a faster exchange rate (0.962 s^{-1} mM^{-1} at 9.36 μs). Markers for the measured Eu^{3+} data are in good agreement with both theoretical Swift–Connick plots. A $\Delta\omega$ of 42.5 ppm was used in both plots, with each Eu^{3+} compound being within ±2 ppm of this value.

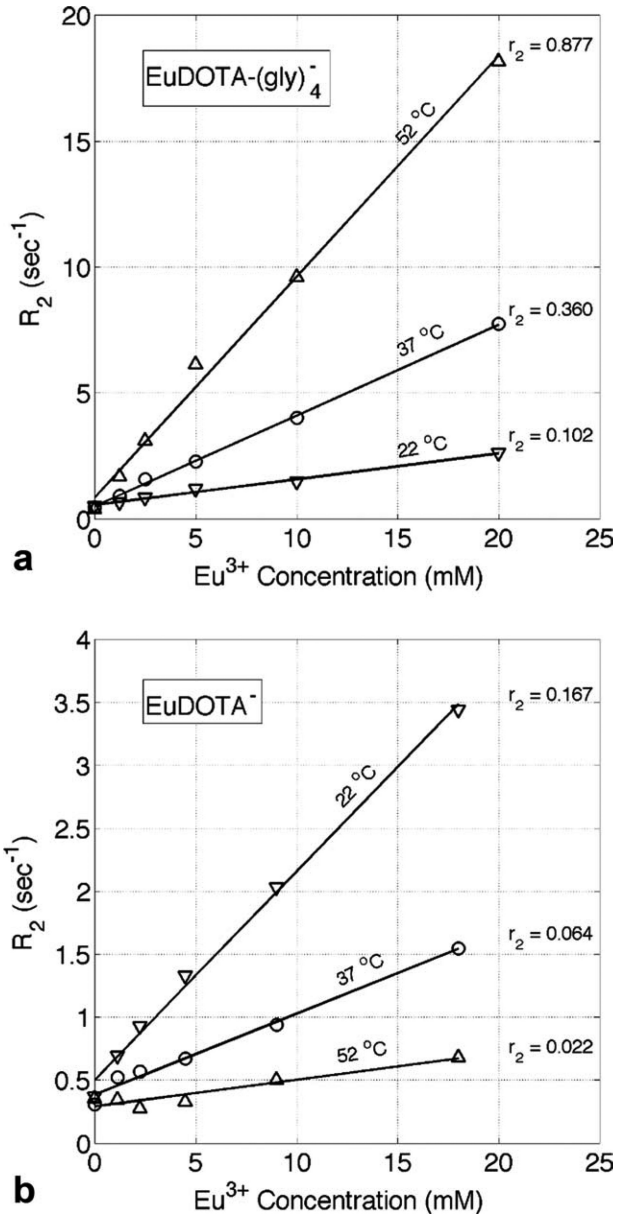

FIG. 3.

a: Transverse relaxation rate (R_2) versus Eu^{3+} concentration (mM) for $EuDOTA\text{-}(gly)_4^-$ at three different temperatures collected at 9.4 T. **b**: A similar plot for $EuDOTA^-$. The r_2 values for each linear fit are given in s^{-1} mM^{-1}. Although r_2 is directly proportional to temperature in (a) it is inversely proportional to temperature in (b) which is consistent with Fig. 2b.

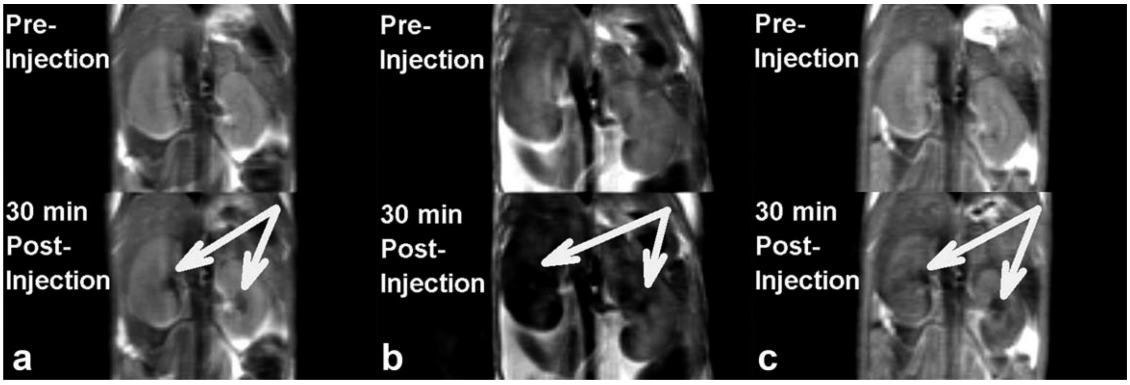

FIG. 4.

Coronal images of mouse kidneys before and after a 0.25-mmol kg^{-1} intravenous injection of (**a**) $EuDOTA^{-}$, (**b**) $EuDOTA\text{-}(gly)_4^{-}$, and (**c**) $EuTETA^{-}$. Although the $EuDOTA^{-}$ (fast exchange) and $EuTETA^{-}$ (no exchange) compounds show minimal renal darkening, the $EuDOTA\text{-}(gly)_4^{-}$ (intermediate exchange) compound shows severe negative contrast due to T_2 exchange.

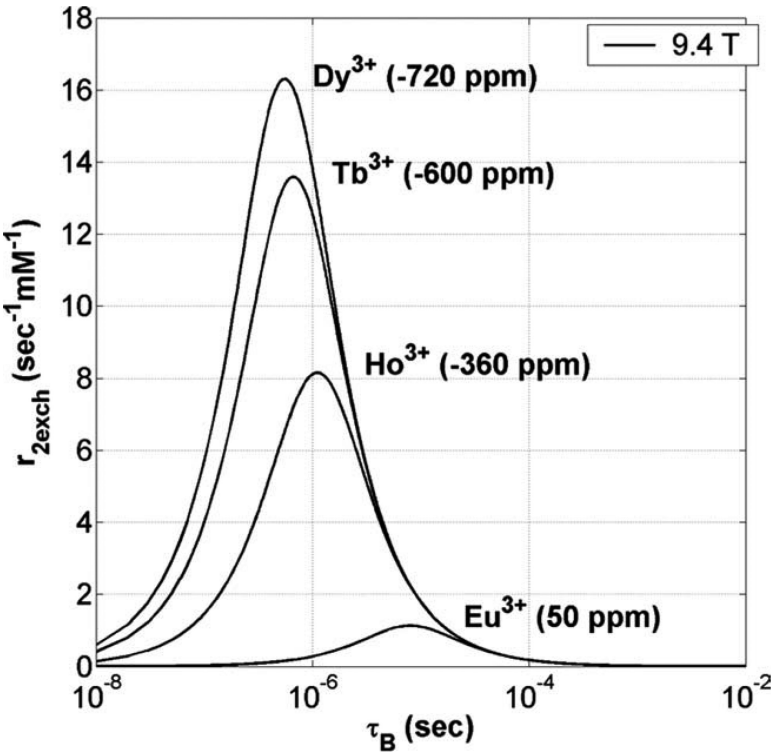

FIG. 5.

A Swift–Connick plot of r_{2exch} versus τ_B for several different paramagnetic lanthanide ions at 9.4 T and 37°C. Each ion has a different $\Delta\omega$ (given in parenthesis) expressed in ppm. As $\Delta\omega$ increases, the maximum r_{2exch} increases and moves toward faster exchange.

Table 1

Water Exchange Properties at 37°C for the Six Different Eu^{3+} Compounds Used in This Study

Eu^{3+} compound	Water exchange rate C_B (s^{-1})	Bound water lifetime τ_B (μs)	Transverse relaxivity at 0.54 T, r_2 (s^{-1} mM^{-1})	Transverse relaxivity at 9.4 T, r_2 (s^{-1} mM^{-1})
$EuDOTA^{-}$	5,000,000	0.2	0.004	0.051
$EuDOTA\text{-}(Me_2gly)_4^{-}$	35,714	28	0.020	0.527
$EuDOTA\text{-}(gly)_4^{-}$	19,231	52	0.035	0.395
$EuDOTA\text{-}(AmPO_2OBu)_4^{-}$	14,085	71	0.043	0.440
$EuDOTA\text{-}(glyOEt)_4^{3+}$	10,000	100	0.050	0.216
$EuTETA^{-}$	0	Simulates infinity	0.001	0.013

C_B ranges from very fast exchange ($EuDOTA^{-}$) to no exchange ($EuTETA^{-}$). Also included are the transverse relaxivity values calculated from Fig. 1a,b.